




The shape of titanium dioxide nanomaterials modulates their protection efficacy against ultraviolet light in human skin cells

Krunoslav Ilić · Atida Selmani · Mirta Milić · Tanja Matijević Glavan · Emilija Zapletal · Marija Ćurlin · Tadahiro Yokosawa · Ivana Vinković Vrček · Ivan Pavičić 

Received: 10 September 2019 / Accepted: 21 February 2020 / Published online: 14 March 2020
© Springer Nature B.V. 2020

Abstract Skin protection against ultraviolet (UV) radiation is necessary to reduce sunburn damage (erythema) and has been recognized as an important preventive measure against the development of cancer. Many sun-blocking pharmaceutical products are based on titanium dioxide nanomaterials (TiO₂ NMs) due to their UV barrier properties. This study aimed to assess if the UV protective efficiency of TiO₂ NMs depends on their shape. We prepared TiO₂ nanowires (TNW), TiO₂ nanotubes (TNT), and TiO₂ nanoplates (TNP) and tested their effects on human keratinocytes before and after

UVB irradiation under in vitro exposure settings. The UVB radiation was applied at the dose equivalent to the UV component observed in one medial erythemal dose. The biological effects of TiO₂ NMs on nonirradiated and UVB-irradiated keratinocytes were observed by means of cell viability, genotoxicity, and inflammatory response. The obtained results clearly showed that the effects of TiO₂ NMs in vitro, either cytotoxic or protective, depend on their shape. These observations highlight the beneficial properties of nanomaterials that can improve the quality and efficacy of nano-enabled

Electronic supplementary material The online version of this article (<https://doi.org/10.1007/s11051-020-04791-0>) contains supplementary material, which is available to authorized users.

K. Ilić · M. Milić · I. V. Vrček · I. Pavičić (✉)
Institute for Medical Research and Occupational Health, Zagreb, Croatia
e-mail: ipavicic@imi.hr

K. Ilić
e-mail: kilic@imi.hr

M. Milić
e-mail: mmilic@imi.hr

I. V. Vrček
e-mail: ivinkovic@imi.hr

A. Selmani · T. M. Glavan · E. Zapletal
Rudjer Boskovic Institute, Zagreb, Croatia

A. Selmani

e-mail: aselmani@irb.hr

T. M. Glavan
e-mail: tglavan@irb.hr

M. Ćurlin
School of Medicine, University of Zagreb, Zagreb, Croatia
e-mail: marija.curlin@mef.hr

T. Yokosawa
Karlsruhe Institute of Technology (KIT), Institute for Nuclear Waste Disposal, Hermann-von-Helmholtz-Platz 1, 76344 Eggenstein-Leopoldshafen, Germany
e-mail: tadahiro.yokosawa@fau.de

T. Yokosawa
Institute of Micro- and Nanostructure Research, Friedrich-Alexander-Universität Erlangen-Nürnberg, Cauerstraße 6, 91058 Erlangen, Germany

products only if the safe-by-design concept has been implemented during the innovation process.

Keywords UVB radiation · Skin · TiO₂ NM · Genotoxicity · Inflammatory response · Viability · Health effects

Introduction

Titanium dioxide (TiO₂) is a metal oxide that occurs in nature in forms of rutile, anatase, or brookite minerals. It is used in many diverse applications, e.g., as a photocatalyst for hydrogen production, in dye-sensitive solar cells, as corrosive-protection coating, gas sensor, white pigment for different materials (papers, plastics, inks, cosmetics), etc. (Baraton 2011; Diebold 2003). Due to its high refractive index, TiO₂ has been also applied in sunscreens to protect the skin from harmful effects of UV radiation (Wright et al. 2017), especially in nanoparticulate form. Nanomaterials (NMs) have in general much greater surface area compared to the same volume of bulk material, thus enabling more efficient interaction with incident UV light (Baraton 2011). However, interaction of TiO₂ NMs with UV light may produce free oxygen radicals that could harm living cells (Long et al. 2007). Such oxidative stress may be mitigated if TiO₂ NMs are coated in sunscreens with silica (SiO₂), dimethicone, or alumina (Al₂O₃) (Wamer et al. 1997; Lademann et al. 2000). Although characterized as biologically inert and approved for use as a food and pharmaceutical additive (Rowe et al. 2009), TiO₂ NMs in cosmetic products may still present safety issues, due to a wide variety of available morphologies, surface coatings, sizes, concentrations, and agglomeration/aggregation states, which may affect their properties and interaction with UV light. Likewise, TiO₂ NMs of various shapes may differ in their toxic potential (Hamilton et al. 2009), but data on the effect of NM shape on their biological properties is scarce. There is also a lack of reliable data on cell penetration and cytotoxicity effects of TiO₂ NMs despite reports on oxidative stress response, modulation of gene expression, and DNA damage in TiO₂ NM-treated human cells (Petković et al. 2011a, b; Gurr et al. 2005). It has been reported that TiO₂ NMs may decrease cell area, proliferation, mobility, and ability to contract collagen in dermal fibroblasts (Pan et al. 2009).

UV radiation occupies the range of 100–400 nm in the electromagnetic radiation spectrum and is divided into UVC (100–280 nm), UVB (280–315 nm), and UVA (315–400 nm) subranges. While UVC is completely absorbed by the ozone layer, UVB and UVA photons are able to reach the Earth's surface and cause acute (erythema, sun tanning) and chronic (skin cancer and photoaging) effects in sufficiently high doses (Popov et al. 2005). The UVA penetrates deep into the dermis, where it can generate ROS and cause indirect DNA damage, while UVB is almost completely absorbed by the epidermis and can cause direct DNA breakage by stimulating the formation of cyclobutane dimers and 6–4 photoproducts (D'Orazio et al. 2013). The UVB may also initiate inflammatory cascade in epidermal keratinocytes resulting in erythema (D'Orazio et al. 2013). Since TiO₂ materials produce ROS when exposed to UV light (Sunada et al. 2003), concerns have been raised whether TiO₂ in sunscreens would compound UV-induced damage and increase the risk of skin cancer, rather than protect from harmful exposure effects. Larger surface area of TiO₂ NMs compared to their bulk counterparts could increase the extent of interaction with UV radiation and the associated hazards. A survey in the Web of Science (WOS) database was performed on December 10th, 2019 to find scientific data on detrimental TiO₂ NM effects on cells (Tables S1–S2 in the Supporting information). The search phrase “TITLE:(“titanium dioxide nanoparticle*” or “tio2 nanoparticle*”) AND (“cytotox*” or “cell tox*”)” returned 76 publications. When the phrase was refined with the TOPIC:“UV” and (“hacat” or “keratinocyt*”) to narrow the search to cell type of interest for this study, only eight publications were found (Table S1 in the Supporting information). Only six of these studies (Table S2 in the Supporting information) have investigated whether the detrimental effect of TiO₂ NMs is exacerbated by subsequent or simultaneous UV exposure (Ghiazza et al. 2014; Ren et al. 2018; Rancan et al. 2014; Park et al. 2011; Zeni et al. 2018; Sharma et al. 2018). Ren et al. (2018) found 50% reduction in the viability of HaCaT cells after 21 h exposure to TiO₂ NPs followed by 1 h irradiation by 365 nm UV light, while TiO₂ NPs did not significantly reduce cell viability by themselves. However, Rancan et al. (2014) reported cell death in UVB-treated HaCaT cells (210 and 630 mJ/cm² doses), but no appreciable difference in cell viability between irradiated cells and cells that were both irradiated and treated with TiO₂

NPs. Their additional analysis of IL-6 release after UVB exposure indicated the beneficial effect of cell pretreatment with TiO₂ NPs (Rancan et al. 2014). In almost all of these studies, the tested TiO₂ NPs were spherical with the exception of polygonal anatase TiO₂ NPs used by Park et al. (2011), but no consideration was given on the effect of nanoparticle shape on cell viability.

We aimed to evaluate the in vitro effect of different TiO₂ NMs on irradiated vs. nonirradiated human skin cells. The TiO₂ NMs were designed to render three different morphologies—TiO₂ nanowires (TNW), TiO₂ nanotubes (TNT), and TiO₂ nanoplates (TNP). Their effect on human keratinocytes (HaCaT) cells was determined by means of cell viability, mitochondrial integrity, inflammatory response, and DNA damage. Exposure conditions included 24 h cell treatment to TiO₂ NMs with or without subsequent exposure to medial erythral dose of UVB irradiation (0.2 kJ/m², 312 nm) (Kuchel et al. 2002), which corresponds to standard erythral dose of 0.1 kJ/m² (CIE CI de l'Eclairage 2000). This study demonstrates for the first time how TiO₂ NMs of different shapes affect irradiated and nonirradiated human skin cells.

Materials and methods

Synthesis of TiO₂ NMs

The TNW and TNT were prepared according to the previously reported protocols (Selmani et al. 2015). Briefly, TNW and TNT powders were prepared using alkaline hydrothermal procedure by suspending 2.0 g of TiO₂ P25 (75% anatase, 25% rutile, Degussa) with aqueous 65 cm³ NaOH solution ($c = 10 \text{ mol dm}^{-3}$). The procedure for TNT and TNW differs in temperature (TNT at 146 °C; TNW at 190 °C) and duration of the synthesis (TNT: $t = 48 \text{ h}$; TNW: $t = 24 \text{ h}$). The TNP were synthesized by the method reported in the work of Han et al. (2009). Titanium (IV) isopropoxide (18 mL, 97% (w/v), Sigma Aldrich, St Louis, MO, USA) was mixed with hydrofluoric acid (2.2 mL, 48% (w/v), Honeywell Riedel de Haën, Thermo Fisher Scientific, Waltham, MA, USA) in a dried Teflon-lined autoclave at 190 °C for 24 h. After the reaction was finished, the obtained precipitates were washed with water thoroughly and incubated with 0.1 mol/L NaOH due to the presence of fluoride impurities that remained after the synthesis until the conductivity and pH were close to values for

deionized water (pH ≈ 6.5 , conductivity $< 10 \mu\text{S cm}^{-1}$). The prepared TiO₂ NM powders were dried at 100 °C for 6 h in the air and stored in glass bottles. In order to remove residual fluoride contamination, powders were calcined in a furnace for 2 h at 500 °C similar to the work of Sofianou et al. (2012).

Stock suspensions of three different TiO₂ NMs were prepared at the concentration of 1000 mg/L by suspending the dry powders in Milli-Q water. The stock suspensions were sonicated for 30 min using a bath sonicator (Grant XUBA1, Wolf Laboratories, Pocklington, UK) to disperse large agglomerates and to obtain a homogeneous suspension. For further characterization (DLS/ELS), sonicated TiO₂ NM stock suspensions were diluted in Milli-Q water or cell culture media. For cell experiments, TiO₂ NMs were diluted from the stock suspensions in Milli-Q water, stirred with a magnetic stirrer, and repeatedly sonicated (1500 V, 20 kHz, Sonicator Ultrasonic Processor XL, Misonix Inc., Farmingdale, NY, USA) for 5 min and stored in glass bottles.

Characterization of TiO₂ NMs

Powder diffraction data for the TNP were collected by the PANalytical X'Pert XCharge diffractometer (Malvern Panalytical, Malvern, UK) in the Bragg–Brentano geometry mode using Cu K α radiation ($\lambda = 0.154056 \text{ nm}$) at room temperature $2\theta = 5\text{--}70^\circ$ with a step size of 0.08° and 10 s per step.

Raman scattering measurements of the TNP were carried out on an EQUINOX 55 device using the Nd-YAG laser ($\lambda = 1064 \text{ nm}$) at room temperature. The Raman spectra were recorded by applying a laser power of 100 mW. The measurement step of the Raman spectrophotometer was 4 cm^{-1} .

Morphology of the TNP was studied by scanning electron microscopy (SEM) and high-resolution transmission electron microscopy (HR-TEM). Morphological studies on NPs have been performed using scanning electron microscopy on a FE-SEM (JEOL JSM-7000F) microscope. TEM specimen was prepared by mixing powder sample with ethanol and dispersing them onto carbon thin films on Cu support grids. The HR-TEM measurements were performed by employing a FEI Tecnai G2 F20 X-TWIN operated at 200 kV. Data analyses were performed by using Digital Micrograph (Gatan Inc., München, Germany).

The specific surface area, s , was determined employing the multipoint Brunauer–Emmett–Teller (BET) method using N_2 as adsorbed gas at 77 K and relative pressure values in the range 0.05–0.3 on a Micromeritics Instrument Corporation, Gemini V series Surface Area Analyzer (Micromeritics Instrument Corporation, Norcross, GA, USA).

Dynamic (DLS) and electrophoretic light scattering (ELS) techniques were used to determine the particles sizes (d_H) and zeta (ζ) potentials, respectively, of TiO_2 NMs suspended in Milli-Q water and cell culture medium for 24 h. Prior to analysis, the samples were diluted 10 times in Milli-Q water from the 1000-mg/L stock solutions. The DLS and ELS measurements were performed using a Zetasizer Nano ZS (Malvern Instruments, UK) equipped with a 532-nm “green” laser. The intensity of scattered light was detected at a back-scattering angle of 173° to reduce multiple scattering as well as the effects of dust. Due to overestimation arising from the scattering of larger particles, d_H values were obtained at peak maximum of the size volume distribution function. Each sample was measured 6 times and the reported results are average values. The ζ potentials of particles were calculated from the measured electrophoretic mobility by means of the Henry equation using the Smoluchowski approximation ($f(\kappa a) = 1.5$). Results are reported as an average value of 3 measurements. The DLS and ELS data processing was done by the Zetasizer software 6.32 (Malvern Instruments, UK).

Cell culture experiments

The HaCaT cells were cultured in high glucose Dulbecco’s modified Eagle’s medium (DMEM) (Sigma Aldrich, St Louis, MO, USA) with addition of 10% heat-inactivated fetal bovine serum (Sigma Aldrich, USA) and 1% penicillin/streptomycin (Sigma Aldrich, USA) in a T75 culture flask (Eppendorf, Hamburg, Germany) until they reached 80% confluency. The culture medium was then removed with a pipette, and cells were washed once with sterile PBS and detached by the addition of 0.25% trypsin–EDTA solution followed by 10 min incubation at $37^\circ C$ and 5% CO_2 . Detached cells were collected, counted on a TC20 automated cell counter (Bio-Rad, Hercules, CA, USA), and seeded in black sterile 96-well plates (Thermo Fisher Scientific, Waltham, MA, USA) at 20,000 cells/well for neutral red uptake (NRU), dichloro-dihydrofluorescein diacetate (DCFH-DA), and Rhodamine 123 (Rh123) assays, or

in clear 6-well plates (Eppendorf, Germany) at 100,000 cells/well for flow cytometry and RT-PCR. For the comet assay, cells were seeded in clear 24-well plates (Eppendorf, Germany) at 100,000 cells/well. Seeded plates were incubated for 24 h at $37^\circ C$ and 5% CO_2 to allow cell attachment. The following day, TiO_2 NMs were added to wells in concentrations 10, 100, and 300 mg/L, while the same volume of sterile Milli-Q water was added to the control cells. After 1 h incubation at $37^\circ C$ and 5% CO_2 , cells were irradiated with 0.2 J of UVB radiation and subsequently incubated for further 24 h at $37^\circ C$ and 5% CO_2 . The source of UVB radiation was a UV crosslinker (Uvitec, Cambridge, UK) CL 508 with 6×8 W tubes and controlled delivery of the UVB dose.

Neutral red uptake assay

Cell culture medium with 5% FBS was prepared and neutral red dye was diluted in the prepared medium to the concentration of 33 mg/L. Following the 24-h HaCaT incubation with TiO_2 NMs, the culture medium was aspirated from plates with a multichannel pipette and cells were washed three times with 200 μL /well of PBS. The prepared neutral red dye solution was added to the plates (100 μL /well), which were then incubated for 3 h at $37^\circ C$ and 5% CO_2 . Desorption medium containing 50% absolute ethanol, 49% deionized sterile H_2O , and 1% glacial acetic acid was prepared. After aspirating neutral red solution from wells, 100 μL /well of desorption medium was added, and the plates were shaken for 10 min on a plate shaker at room temperature. Absorbance was read by Victor3™ multilabel plate reader (Perkin Elmer, Waltham, MA, USA) at the wavelength of 530 nm.

Mitochondrial membrane leakage assay

To evaluate mitochondrial membrane leakage in HaCaT cells after TiO_2 NMs treatment and/or irradiation, Rh123 dye was used. After incubation with TiO_2 NMs, culture medium was removed from wells, cells were washed twice with 200 μL /well of PBS and 100 μL /well of Rh123 dye (1 mg/L in PBS) was added to wells. Plates were incubated for 30 min at $37^\circ C$ and 5% CO_2 and fluorescence intensity was detected by Victor3™ multilabel plate reader at an excitation wavelength of 485 nm and an emission wavelength of 535 nm.

Flow cytometry experiments

Flow cytometry was used to determine cell viability and mitochondrial membrane integrity of treated HaCaT cells. After TiO₂ NM treatment and/or irradiation, supernatants were collected from wells into 2 mL tubes (Eppendorf, Germany), after which cells were washed twice with 1 mL/well of sterile PBS. Washed cells were detached by adding 200 µL/well of 0.25% trypsin–EDTA solution and incubating for 10 min at 37 °C and 5% CO₂. Afterwards, 500 µL/well of cell culture medium was added, and the detached cells were collected with a pipette and pooled with supernatants from the same well in order to collect both dead and viable cells from the same sample.

Samples were centrifuged at 800×*g* for 5 min at room temperature and resuspended in 1 mL PBS + 2% BSA per sample. After 30 min incubation at room temperature, cells were again centrifuged at 800×*g* for 5 min, and the tubes were inverted to remove the supernatant (cells in approximately 100 µL PBS remained in the tubes). The collected cells were stained with propidium iodide (PI) to count dead cells or Rh123 to evaluate mitochondrial membrane leakage. To each sample, 5 µL of 50 µg/mL PI solution was added (final concentration 2.5 µg/mL). Samples were incubated for 10 min at room temperature in the dark. After PI staining, cells were additionally stained with Rh123 (final concentration 2.62 µM).

After staining, 2 mL/sample of PBS was added to the tubes, and samples were centrifuged at 800×*g* for 5 min at room temperature. After removing the supernatants, samples were washed again with PBS and 250 µL was left in the tubes. Samples were acquired immediately on Attune NxT flow cytometer (Thermo Fisher Scientific, USA).

Inflammatory response

Inflammatory response in HaCaT cells treated with TiO₂ NMs and/or irradiated with UVB light for 24 h was evaluated by the RNA expression analysis of interleukin 6 (IL-6), tumor necrosis factor α (TNFα), interleukin 1β (IL-1β), and matrix metalloproteinase-1 (MMP1) using the real-time PCR method. The RNA was isolated using *RNeasy*PLUS Mini Kit (Qiagen, Hilden, Germany). The amount of 0.6 µg of RNA was then used as a template in cDNA synthesis reaction by High Capacity cDNA Reverse Transcription Kits (Applied Biosystems,

Branchburg, NJ, USA). The PCR reactions were performed with Sybr® Green PCR Master Mix (Applied Biosystems, USA) on a CFX96™ Real-Time PCR Detection System (Bio-Rad, USA) with the following program: 95 °C for 10 min (initial denaturation), 95 °C for 30 s (denaturation), and 62 °C for 30 s and 60 °C for 30 s (annealing and elongation). Primers used to amplify cDNA were as follows: IL-6-F 5'-TGCG TCCGTAGTTTCCTTCT-3', IL-6-R 5'-GCCT CAGACATCTCCAGTCC-3'; TNFα-F 5'-GAGC ACTGAAAGCATGATCC-3', TNFα-R 5'-CGAG AAGATGATCTGACTGCC-3'; IL-1β-F 5'-AAAC AGATGAAGTGCTCCTTCC-3', IL-1β-R 5'-AAGA TGAAGGGAAAGAAGGTGC-3'; MMP1-F 5'-GGGAGATCATCGGGACAACCTC-3', MMP1-R 5'-GGGCCTGGTTGAAAAGCAT-3'; and arp-F 5'-TTGCGGACACCCTCCAGGAAGC-3', arp-R 5'-GGCACCATTGAAATCCTGAGTGATGTG-3'.

All data were analyzed using the 2^{-ΔΔCt} (relative quantitation) method, after ensuring that all primer sets amplified their respective sequence targets with similar efficiencies and without primer–dimers. Arp was used as a reference gene.

Alkaline comet assay

Alkaline comet assay was performed to quantify the extent of DNA damage caused by UVB and/or TiO₂ NM treatments following previously developed protocols (Collins 2004; Milić et al. 2015). Cells were seeded in 24-well plates (1 × 10⁵ cells/mL) and treated with the concentration range from 1 to 150 mg/L of TiO₂ NMs for 24 h. Prior to treatment, the cells were incubated in serum-free media for 12 h (in order to synchronize the cell cycle phases). After the treatment, cells were detached by the use of 1 mL of trypsin and resuspended in 300 µL of DMEM high glucose medium with FBS included (1:1) for trypsin deactivation. Cells were centrifuged at 70×*g* for 8 min. The supernatant was removed and 100 µL of DMEM medium was added. Aliquots of 10 µL of this suspension were mixed with 100 µL of 0.5% low-melting agarose, and the suspension was placed on slides precoated with 200 µL of 1% normal-melting agarose. Slides were allowed to solidify on ice for 10 min and were kept in prechilled lysis solution (2.5 M NaCl, 100 mM Na₂EDTA, 10 mM Tris, pH = 10, 1% sodium sarcosinate, 1% Triton X-100, 10% dimethyl sulfoxide) at 4 °C. After 1 h, the slides were placed in freshly prepared denaturation and

electrophoresis buffer (10 mM NaOH, 200 mM Na₂EDTA, pH = 13), incubated for 20 min at 4 °C, and electrophoresed for 20 min at 25 V and 300 mA. Finally, the slides were neutralized three times, 5 min each time, in 0.4 M Tris buffer (pH 7.5) and then dehydrated with ethanol (two incubations with 70% and one with 96% ethanol, for 10 min each). The slides were kept in a humid atmosphere in the dark at 4 °C until further analysis. For image analysis, slides were stained with 100 µL of 20 µg/mL ethidium bromide (Sigma Aldrich, USA) solution for 10 min. A minimum of 100 randomly selected DNA molecules per sample (50 comets per slide) were scored. Comets were randomly captured at a constant depth of the gel, avoiding the edges of the gel, occasional dead cells, and DNA near or trapped in an air bubble and superimposed comets. Slides were scored using an image analysis system (Comet Assay II; Perceptive Instruments Ltd., Bury St Edmunds, UK) attached to a fluorescence microscope (Zeiss, Jena, Germany), equipped with the appropriate filters. The parameters selected for the quantification of DNA damage were comet tail length (in µm) and tail intensity (% of DNA in tail). The extent of DNA damage, as recorded by the alkaline comet assay, was analyzed considering the mean (\pm standard deviation of the mean), median, and range of the comet parameters measured.

Statistical analysis

Statistical analyses for flow cytometry, mitochondrial membrane leakage assay, RT-PCR, and alkaline comet assay were performed in GraphPad Prism 6 (GraphPad Software, San Diego, CA, USA). Results from each test were analyzed using one-way ANOVA with multiple comparison test, where all treatment groups were individually compared to both control groups (nonirradiated and UVB-irradiated cells). Significance threshold for all analyses was set at $P < 0.05$. Mean values and standard deviations for all sample groups were calculated and plotted using GraphPad Prism software.

Results

Characterization and stability evaluation of TiO₂ NMs

The detailed characterization of TNW and TNT was previously reported in the work of Selmani et al.

(2015). The PXRD pattern for the TNP corresponds to the typical PXRD pattern of the TiO₂ anatase crystal form (JCPDS 21-1272) as shown in Fig. 1a. Raman spectroscopy was applied to characterize the TNP (Fig. 1b).

The characteristic bands 142.8, 395.4515.1, and 637.6 cm⁻¹ were in good agreement with the literature data (Tian et al. 2012) and consistent with the PXRD data. The TNP was visualized by the SEM and TEM micrographs (Fig. 2) that showed a plate-like structure. The HR-TEM analyses of the TNP samples have shown that the length of TNP is \approx 100 nm while its width is \approx 35 nm.

The physicochemical properties of the TNMs were determined by means of hydrodynamic diameter, surface charge, and BET surface area analysis. The specific surface areas for TNW, TNT, and TNP were 28.5, 314.5, and 21.8 m²/g, respectively. The significantly higher specific surface area of TNT can be attributed to their layered, tube-like structure with internal cavities, as was previously discussed by Selmani et al. (2015). The DLS and ELS data are summarized in Table 1. DLS measurements revealed monomodal size distribution for all TiO₂ NMs in Milli-Q water with average d_H values of 350, 110, and 190 nm for TNW, TNT, and TNP, respectively. Significant TiO₂ NM agglomeration occurred in the cell culture medium due to the increase of ionic strength of the medium although ζ potential values did not change significantly.

Cell viability and mitochondrial membrane integrity

Viability of TiO₂ NM-treated and/or irradiated HaCaT cells was measured by the NRU assay. The obtained results showed an increase in absorbance values with increasing TiO₂ NM concentration, in both nonirradiated and irradiated samples (Fig. 3a). The apparent increase in signal was lower for TNT compared to TNW and TNP, but dose-dependent for all TiO₂ NMs. However, there was no difference in absorbance between irradiated and nonirradiated TiO₂ NM-treated samples, as well as between TiO₂ NM-treated cells and TiO₂ NMs in cell-free culture medium at the concentrations tested (Fig. 3a). Such results clearly indicated interferences of TiO₂ NMs with the readout at 530 nm that masked any UVB- or TiO₂ NM-related effects on HaCaT viability.

We have already evidenced similar interferences for other types of NMs (Vinković Vrček et al. 2015; Pem

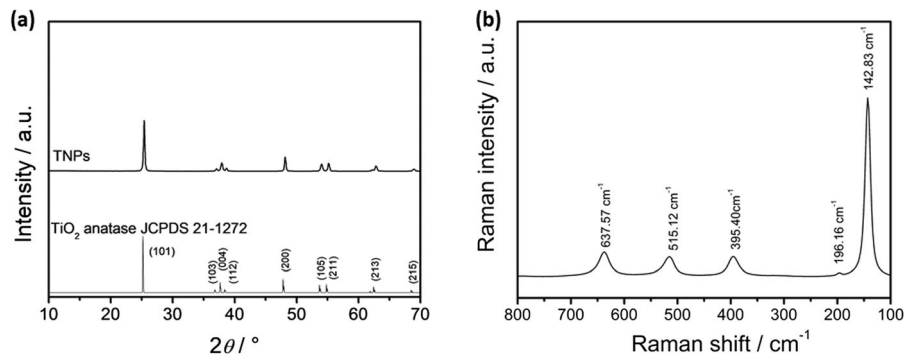


Fig. 1 **a** Powder X-ray diffraction patterns of the TNP. Pure anatase crystal form is provided from the Inorganic Crystal Structure Database (JCPDS 21-1272). **b** Raman spectra of the TNP sample

et al. 2018). The TNW and TNP showed higher interferences than TNT. Unfortunately, we were not able to diminish TiO_2 NM interferences in a plate reader experimental setup by any modifications of the *in vitro* protocol. Similar interferences were also observed for Rh123 assay as presented in Fig. 3b. We observed dose-dependent interferences for both assays (NRU and Rh123) as measured by the microplate reader. For all TiO_2 NM types, the threshold concentration for interference with fluorescence and absorbance readouts was demonstrated to be above 10 mg/L, as already reported elsewhere (Kroll et al. 2012). Consequently, results obtained in these assays are not reliable as the cellular effects of TiO_2 NMs cannot be distinguished from these interferences. To overcome this problem, the flow cytometry technique was used for PI- and Rhodamine 123-stained cells that was able to distinguish signals originating from TiO_2 NMs from the cell signals (Fig. 4). Flow cytometry presents an advantage over plate-based assays because NPs remaining in the sample

can be excluded from the analyzed results in the FSC/SSC plot based on their size.

Flow cytometry experiments using PI staining provided an accurate gauge of TiO_2 NM cellular effects and revealed that all three types of TiO_2 NMs were not cytotoxic up to the highest tested concentration, i.e., 300 mg/L. Moreover, results presented in Fig. 4a indicated the protective role of TNP and TNW at the highest applied dose, while TNT did not protect the viability of UVB-irradiated HaCaT cells. Analysis of results obtained after Rh123 staining (Fig. 4b) revealed a dose-response increase in mitochondrial activity of cells treated with TiO_2 NMs compared to the cells that were irradiated by UVB but not exposed to TiO_2 NMs. As in the case of PI assay, the TNP and TNW demonstrated a protective role for mitochondrial membrane integrity after UVB irradiation in a dose-dependent manner, while TNT-treated cells were in the same conditions as the control, nontreated cells (Fig. 4b). Thus, the highest tested concentration of

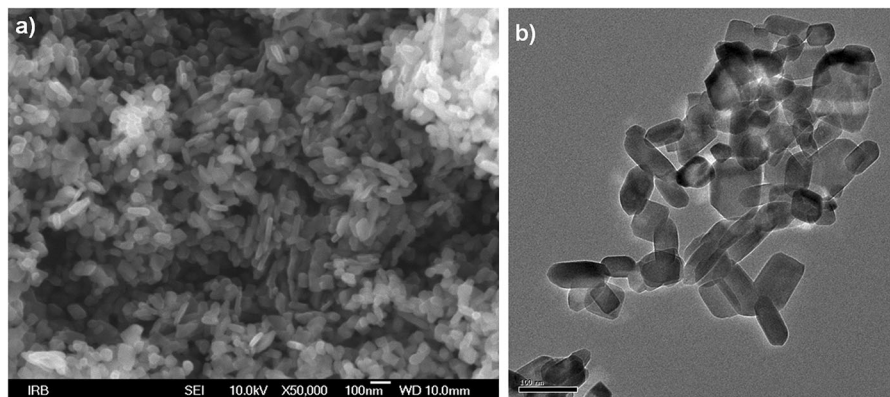


Fig. 2 **a** SEM and **b** TEM micrographs of TiO_2 nanoplates (TNP)

Table 1 Hydrodynamic diameter (d_H in nm) obtained from size volume-weighted distribution and ζ potential values (in mV) of TiO₂ nanowires (TNW), nanotubes (TNT), and nanoplates (TNP)

NM type	Milli-Q water			Cell culture medium		
	d_H /nm	% mean volume	ζ /mV	d_H /nm	% mean volume	ζ /mV
TNW	348.4 ± 42.7	100	-23.6 ± 0.8	225.2 ± 45.6 817.9 ± 140.2	2.4 97.6	-18.7 ± 0.8
TNT	109.4 ± 72.0	100	-14.3 ± 0.5	895.7 ± 209.0	100	-13.8 ± 1.5
TNP	189.4 ± 58.9	100	-18.4 ± 1.1	901.6 ± 86.3	100	-19.8 ± 0.6

TNW and TNP preserved cellular viability and mitochondrial membrane potential, whereas nanotubes did not shield cells from the UV-induced cell damages and death.

Inflammatory response

Exposure of HaCaT cells to UVB light significantly upregulated the expression of all four tested inflammation-associated genes (Fig. 5 and Table 2).

The UV-mediated increase in IL-1 β expression was reduced by treatment with 100 mg/L TNP, with 300 mg/L of TNT, and with 100 and 300 mg/L of TNW. The anti-inflammatory effect was even more pronounced in MMP1 expression analysis, where all tested TiO₂ NMs, except 100 mg/L TNT, significantly downregulated mRNA levels compared to UVB-treated control cells. IL-6 analysis yielded similar results, where all TiO₂ NMs, except 100 mg/L TNP, reduced the UVB-associated upregulation. TNF α expression induced by UVB irradiation was diminished in cells treated with TNP and TNT applied at the 300-mg/L concentration.

in Milli-Q water and cell culture medium at 25 °C and TiO₂ NM mass concentrations of 100 mg/L

Taken together, the gene expression analysis has shown that TiO₂ NMs had a protective role and reduced the extent of UVB-induced inflammation in HaCaT cells in a dose-dependent manner.

Genotoxicity

Alkaline comet assay was used to quantify the extent of DNA damage caused by TiO₂ NM treatment. Cells were immobilized in agarose gel, lysed with detergent, and exposed to an electric field. DNA molecules that were damaged by single- or double-stranded breaks lost their supercoiled structures and extended toward the anode, resulting in a comet-like tail of DNA extending from immobilized nuclei. Two endpoints of alkaline comet assay were analyzed in treated HaCaT cells: tail length and tail intensity that both positively correlate with the extent of DNA damage (Fig. 6).

Both parameters were increased in UVB-irradiated cells compared to nonirradiated control HaCaT cells (Fig. 6). This was a clear sign that exposure to UVB light negatively affected cellular integrity, which was supported by data on cell mortality obtained after PI cell staining (Fig. 4a). TiO₂ NM treatment alone slightly

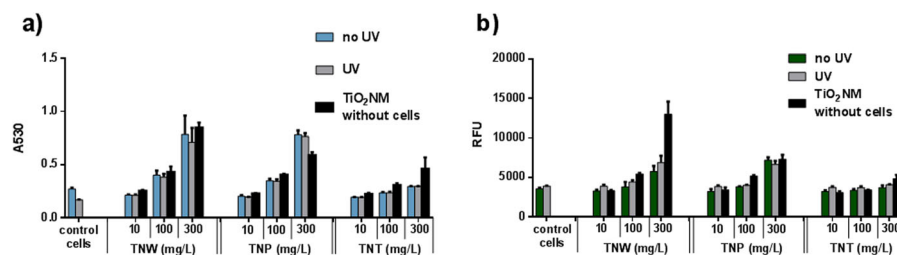


Fig. 3 Effect of UVB irradiation and TiO₂ NM treatment **a** results of neutral red uptake (NRU) assay to determine TiO₂ NM effect on cell viability and **b** on Rhodamine 123 (Rh123) fluorescence in HaCaT cells measured using a plate reader. Data from microplate

reader measurements are given as absorbance for NRU assay or read fluorescence unit (RFU) values for Rh123 assay. Data represent average values obtained from three independent experiments, while standard deviations are given as error bars

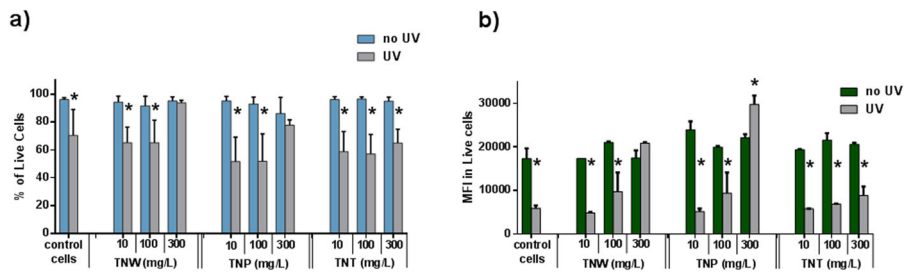


Fig. 4 Effect of UVB irradiation and TiO₂ NM treatment on a mortality of HaCaT cells as determined by the propidium iodide (PI) staining and on b Rhodamine 123 (Rh123) fluorescence in HaCaT cells, both measured by a flow cytometer. Data for PI assay are given as % of live cells and as MFI (mean fluorescence

intensity) values for Rh123 staining. Data represent average values of three independent experiments, while standard deviations are given as error bars. Significant differences from control cells (non-UV-irradiated) are denoted with asterisk (*P* < 0.05)

increased tail length and tail intensity compared to non-UVB-irradiated control cells, and the effect was most pronounced in cells treated with 150 mg/L of TNP. However, consistent with all the above presented results, TiO₂ NM treatment reduced DNA damages in UVB-irradiated cells (Fig. 6). Results for tail intensity also showed that TiO₂ NM-exposed cells had a lower percentage of damaged DNA compared to UVB-irradiated control cells.

Discussion

TiO₂ NMs are a group of materials growing in importance and diversity of application, already routinely used in topically applied cosmetic products. Nonetheless,

there are still existing knowledge gaps on their interactions with living systems, namely, the influence of their diverse physicochemical properties like shape on skin cells, particularly after skin exposure to UV light. The literature survey (performed on December 10th, 2019) revealed reports on the ability of TiO₂ NMs to induce oxidative stress, mitochondrial damage, and subsequent apoptotic or autophagic pathway activation on various types of cell lines, including rat cardiomyoblasts (Huerta-García et al. 2018), human erythrocytes (Khan et al. 2015; Li et al. 2008), mouse fibroblasts (Jin et al. 2008), human nonsmall cell lung cancer cells (A549) (Wang et al. 2015), HeLa cells (Ramkumar et al. 2012), D145 cells (He et al. 2017), and more. Only Ma et al. (2017) evaluated the shape-related effects of TiO₂ NMs (nanotubes vs. anatase crystalline structure) on human

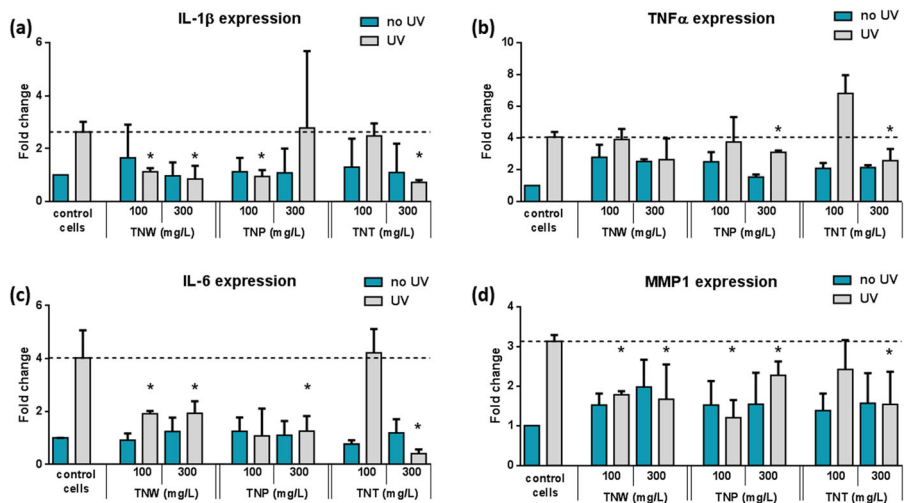


Fig. 5 The expression of pro-inflammatory cytokines (IL-1β, TNFα, and IL-6) and MMP1 in HaCaT cells after treatment with UV light and TiO₂ NMs. Dashed lines denote values of gene expression fold change in UV-irradiated control cells. Asterisks

denote samples where TiO₂ NM treatment significantly reduced gene expression that was elevated by UV treatment, indicating protective TiO₂ NM effect (*P* < 0.05)

Table 2 Effects of TiO₂ NMs on pro-inflammatory gene expression in UVB-exposed HaCaT cells. Treatments that significantly reduced the UVB-stimulated gene expression are marked with +

		Gene downregulation relative to UV-treated cells				
		IL-1 β	MMP1	TNF α	IL-6	
TiO ₂ NMs (mg/L)	Wires	100	+	+	-	+
		300	+	+	-	+
	Plates	100	+	+	-	-
		300	-	+	+	+
	Tubes	100	-	-	-	-
		300	+	+	+	+

bronchial epithelial cells (16HBE) and A549 cells, but reported that that cytotoxic effect is dependent on the NM size and concentration, as well as on the cell type, rather than the NM shape. Reports on the role of TiO₂ NMs in cell protection against UV irradiation are even scarcer. Our study evaluated for the first time the role of shape, as one of the important NM physicochemical properties, on the potential protective action of TiO₂ NMs against UV irradiation.

We have prepared TiO₂ TNW, TNT, and TNP that differed in interactions with HaCaT cells and UV light. Our results demonstrated that the biological effects of TiO₂ NMs depend on their shape. Cell mortality measured by PI staining showed lower percentages of dead cells when UVB-irradiated HaCaT cells were pretreated with TNW and TNT. A similar protective role of these two TiO₂ NM types was also demonstrated by Rh123 staining. The same pretreatment with TNW and TNT also preserved mitochondrial integrity of UVB-exposed keratinocytes. Such effects were not observed in HaCaT cells treated with the same concentration of TNP. Therefore, TiO₂ NM shape may play a decisive role in their interaction with UVB light and subsequent skin protective action against UVB irradiation.

The results from the comet assay confirmed that UVB irradiation damaged keratinocytes by disrupting the integrity of cellular DNA. Thus, DNA damage may be one of the main reasons for reduced cell viability of UVB-irradiated HaCaT cells compared to nonirradiated cells. Although TiO₂ NM treatment alone slightly increased DNA damage, this effect was decreased in UVB-exposed cells.

Furthermore, the expression of inflammation-linked genes in UVB-exposed and TiO₂ NM-treated keratinocytes confirmed a shape-dependent protective role of TiO₂ NMs. UVB exposure expectedly increased the expression of all tested genes in HaCaT cells, as it was previously shown that UV initiated the inflammatory cascade in keratinocytes (Yoshizumi et al. 2008; Bashir et al. 2009) with carcinogenic potential (Kim and He 2014). Generally, all three types of TiO₂ NMs achieved reduction in expression of tested inflammation markers, particularly at the highest dose. The TiO₂ NMs themselves did not increase the expression of any of the four tested genes, so the inflammatory response in keratinocytes can be conclusively linked to UVB irradiation alone. Indeed, 300 mg/L concentrations of TNW and TNP downregulated three out of four genes, significantly reducing the potency of inflammatory cascade. This effect possibly contributed to preservation of cell viability and mitochondrial integrity that were determined by flow cytometry.

Considering that all three TiO₂ NM types had similar size and ζ potential in cell culture medium, the only salient differences remained their shape and the resulting specific surface area. TNT were shown to have ~ 10 times greater surface area compared to TNW and TNP, which should allow more interaction with incident radiation and, presumably, a greater protective effect for underlying skin cells. However, the opposite was shown to be the case. Both the TNW and TNP, applied at a dose of 300 mg/L, blocked the cytotoxic effects of UVB irradiation and preserved cell viability and mitochondrial function of

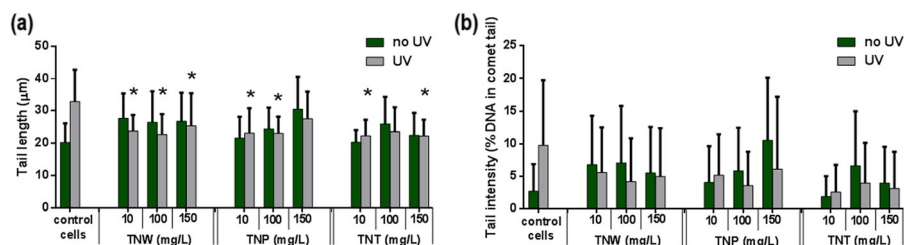


Fig. 6 DNA damage induced by UVB light and/or different TiO₂ NMs in HaCaT cells. Asterisk (*) denotes TiO₂ NM- and UV-treated cells that had significantly shorter DNA tail length compared to UV-irradiated control cells ($P < 0.05$)

HaCaT cells, but TNT did not show such property. Although TNT inhibited an inflammatory response in UVB-treated keratinocytes, this was not enough to protect cells from UVB-induced cell death. One possible explanation is the production of free oxygen radicals by TiO₂ NMs exposed to UV as reported by Long et al. (2007). Whereas this effect is mitigated in sunscreens using TiO₂ by silica or dimethicone coating, TiO₂ NMs used here were uncoated and potentially contributed to cellular oxidative stress. Moreover, greater specific surface area of TNT compared to the other two TiO₂ NM types would in this case increase oxidative stress and hinder cell viability, as was seen here. Further studies are needed to obtain a more detailed picture of interplay between cells, TiO₂ NMs, and UV radiation and determine the precise mechanism of their interaction.

Conclusions

Exposure to UV radiation presents a persistent risk for development of acute and chronic skin pathologies, including metastatic melanoma. To protect the skin from adverse UV effects, nanotechnology may provide efficient and safe solutions like TiO₂ NMs to be used in skin protection cosmetics. This work demonstrated that the shape of TiO₂ NMs is an important property that has to be considered in the design of UV protective nano-enabled products. We have tested TiO₂-based nanowires, nanoplates, and nanotubes. The obtained results showed that nanowires and nanoplates reduced the extent of UVB-induced damage to cellular viability and mitochondrial membrane integrity, as well as downregulated the expression of pro-inflammatory cytokines of human skin cells. In comparison, nanotubes were much less effective in protecting cells from detrimental UVB effects. This work underscores that modification of NM shape can open new possibilities to tailor nanotechnological tools for specific purposes, and increase their importance and applicability.

Funding information This manuscript was supported by the Croatian Science Foundation [grant number HRZZ-IP-2016-06-2436].

Compliance with ethical standards

Conflict of interest The authors declare that they have no conflict of interest

References

- Baraton MI (2011) Nano-TiO₂ for solar cells and photocatalytic water splitting: scientific and technological challenges for commercialization. *Open Nanosci J* 5:64–77. <https://doi.org/10.2174/1874140101105010064>
- Bashir MM, Sharma MR, Werth VP (2009) TNF- α production in the skin. *Arch Dermatol Res* 301:87–91. <https://doi.org/10.1007/s00403-008-0893-7>
- CIE CI de Éclairage (2000) Erythema reference action spectrum and standard erythema dose. CIE ISO 171661999(E)/CIE S 007-1998, 4
- Collins AR (2004) The comet assay for DNA damage and repair: principles, applications, and limitations. *Mol Biotechnol* 26(3):249–261. <https://doi.org/10.1385/MB:26:3:249>
- D’Orazio J, Jarrett S, Amaro-Ortiz A, Scott T (2013) UV radiation and the skin. *Int J Mol Sci* 14:12222–12248. <https://doi.org/10.3390/ijms140612222>
- Diebold U (2003) The surface science of titanium dioxide. *Surf Sci Rep* 43:53–229. [https://doi.org/10.1016/s0167-5729\(02\)00100-0](https://doi.org/10.1016/s0167-5729(02)00100-0)
- Ghiazza M, Alloa E, Oliaro-Bosso S, Viola F, Livraghi S, Rembes D, Capomaccio R, Rossi F, Ponti J, Fenoglio I (2014) Inhibition of the ROS-mediated cytotoxicity and genotoxicity of nano-TiO₂ toward human keratinocyte cells by iron doping. *J Nanopart Res* 16:2263–2217. <https://doi.org/10.1007/s11051-014-2263-z>
- Gurr JR, Wang ASS, Chen CH, Jan KY (2005) Ultrafine titanium dioxide particles in the absence of photoactivation can induce oxidative damage to human bronchial epithelial cells. *Toxicology* 213:66–73. <https://doi.org/10.1016/j.tox.2005.05.007>
- Hamilton RF, Wu N, Porter D, Buford M, Wolfarth M, Holian A (2009) Particle length-dependent titanium dioxide nanomaterials toxicity and bioactivity. *Part Fibre Toxicol* 6: 35. <https://doi.org/10.1186/1743-8977-6-35>
- Han X, Kuang Q, Jin M, Xie Z, Zheng L (2009) Synthesis of titania nanosheets with a high percentage of exposed (001) facets and related photocatalytic properties. *J Am Chem Soc* 131(9):3152–3153. <https://doi.org/10.1021/ja8092373>
- He F, Yu W, Fan X, Jin B (2017) In vitro cytotoxicity of biosynthesized titanium dioxide nanoparticles in human prostate cancer cell lines. *Trop J Pharm Res* 16(12):2793–2799. <https://doi.org/10.4314/tjpr.v16i12.2>
- Huerta-García E, Zepeda-Quiroz I, Sánchez-Barrera H, Colín-Val Z, Alfaro-Moreno E, Del M, Ramos-Godínez P, López-Marure R (2018) Molecules internalization of titanium dioxide nanoparticles is cytotoxic for H9c2 rat cardiomyoblasts. *Molecules* 23:1955. <https://doi.org/10.3390/molecules23081955>
- Jin CY, Zhu BS, Wang XF, Lu QH (2008) Cytotoxicity of titanium dioxide nanoparticles in mouse fibroblast cells. *Chem Res Toxicol* 21:1871–1877. <https://doi.org/10.1021/tx800179f>
- Khan M, Naqvi AH, Ahmad M (2015) Comparative study of the cytotoxic and genotoxic potentials of zinc oxide and titanium dioxide nanoparticles. *Toxicol Rep* 2:765–774. <https://doi.org/10.1016/j.toxrep.2015.02.004>

- Kim Y, He YY (2014) Ultraviolet radiation-induced non-melanoma skin cancer: regulation of DNA damage repair and inflammation. *Genes Dis* 1(2):188–198. <https://doi.org/10.1016/j.gendis.2014.08.005>
- Kroll A, Pillukat MH, Hahn D, Schnekenburger J (2012) Interference of engineered nanoparticles with in vitro toxicity assays. *Arch Toxicol* 86:1123–1136. <https://doi.org/10.1007/s00204-012-0837-z>
- Kuchel JM, Barnetson RSC, Halliday GM (2002) Ultraviolet a augments solar-simulated ultraviolet radiation-induced local suppression of recall responses in humans. *J Invest Dermatol* 118:1032–1037. <https://doi.org/10.1046/j.1523-1747.2002.01773.x>
- Lademann HJ, Weigmann Schäfer G, Müller W, Sterry JH, Jürgen Lademann PD (2000) Investigation of the stability of coated titanium microparticles used in sunscreens. *Skin Pharmacol Appl Ski Physiol* 13:258–264. www.karger.com/journals/sph. Accessed 6 June 2019
- Li SQ, Zhu RR, Zhu H, Xue M, Sun XY, De Yao S, Wang SL (2008) Nanotoxicity of TiO₂ nanoparticles to erythrocyte in vitro. *Food Chem Toxicol* 46:3626–3631. <https://doi.org/10.1016/j.fct.2008.09.012>
- Long TC, Tajuba J, Sama P, Saleh N, Swartz C, Parker J, Hester S, Lowry GV, Veronesi B (2007) Nanosize titanium dioxide stimulates reactive oxygen species in brain microglia and damages neurons in vitro. *Environ Health Perspect* 115:1631–1637. <https://doi.org/10.1289/ehp.10216>
- Ma Y, Guo Y, Wu S, Lv Z, Zhang Q, Ke Y (2017) Titanium dioxide nanoparticles induce size-dependent cytotoxicity and genomic DNA hypomethylation in human respiratory cells. *RSC Adv* 7:23560. <https://doi.org/10.1039/c6ra28272e>
- Milić M, Leitinger G, Pavičić I, Zebić Avdičević M, Dobrović S, Goessler W, Vinković Vrček I (2015) Cellular uptake and toxicity effects of silver nanoparticles in mammalian kidney cells. *J Appl Toxicol* 35(6):581–592. <https://doi.org/10.1002/jat.3081>
- Pan Z, Lee W, Slutsky L, Clark RAF, Pernodet N, Rafailovich MH (2009) Adverse effects of titanium dioxide nanoparticles on human dermal fibroblasts and how to protect cells. *Small* 5(4):511–520. <https://doi.org/10.1002/sml.200800798>
- Park HO, Yu M, Kang SK, Yang SI, Kim YJ (2011) Comparison of cellular effects of titanium dioxide nanoparticles with different photocatalytic potential in human keratinocyte, HaCaT cells. *Mol Cell Toxicol* 7:67–75. <https://doi.org/10.1007/s13273-011-0010-4>
- Pem B, González-Mancebo D, Moros M, Ocaña M, Becerro AI, Pavičić I, Selmani A, Babić M, Horák D, Vinković Vrček I (2018) Biocompatibility assessment of up- and down-converting nanoparticles: implications of interferences with in vitro assays. *Methods Appl. Fluoresc.* 7(1):014001. <https://doi.org/10.1088/2050-6120/aae9c8>
- Petković J, Kuzma T, Rade K, Novak S, Filipič M (2011a) Pre-irradiation of anatase TiO₂ particles with UV enhances their cytotoxic and genotoxic potential in human hepatoma HepG2 cells. *J Hazard Mater* 196:145–152. <https://doi.org/10.1016/j.jhazmat.2011.09.004>
- Petković J, Žegura B, Stevanović M, Dmrović N, Uskoković D, Novak S, Filipič M (2011b) DNA damage and alterations in expression of DNA damage responsive genes induced by TiO₂ nanoparticles in human hepatoma HepG2 cells. *Nanotoxicology* 5(3):341–353. <https://doi.org/10.3109/17435390.2010.507316>
- Popov AP, Lademann J, Priezzhev AV, Myllylä R (2005) Effect of size of TiO₂ nanoparticles embedded into stratum corneum on ultraviolet-A and ultraviolet-B sun-blocking properties of the skin. *J Biomed Opt* 10(6):064037. <https://doi.org/10.1117/1.2138017>
- Ramkumar KM, Manjula C, Gnanakumar G, Kanjwal MA, Sekar TV, Paulmurugan R, Rajaguru P (2012) Oxidative stress-mediated cytotoxicity and apoptosis induction by TiO₂ nanofibers in HeLa cells. *Eur J Pharm Biopharm* 81:324–333. <https://doi.org/10.1016/j.ejpb.2012.02.013>
- Rancan F, Nazemi B, Rautenberg S, Ryll M, Hadam S, Gao Q, Hackbarth S, Haag SF, Graf C, Rühl E, Blume-Peytavi U, Lademann J, Vogt A, Meinke MC (2014) Ultraviolet radiation and nanoparticle induced intracellular free radicals generation measured in human keratinocytes by electron paramagnetic resonance spectroscopy. *Skin Res Technol* 20:182–193. <https://doi.org/10.1111/srt.12104>
- Ren Y, Liu X, Geng R, Lu Q, Rao R, Tan X, Yang X, Liu W (2018) Increased level of A2,6-sialylated glycans on HaCaT cells induced by titanium dioxide nanoparticles under UV radiation. <https://doi.org/10.3390/nano8040253>
- Rowe RC, Sheskey PJ, Owen SC (2009) Handbook of pharmaceutical excipients, 6th edn. Pharmaceutical Press, London, pp 741–744
- Selmani A, Špadina M, Plodinec M, Delač Marion I, Willinger MG, Lützenkirchen J, Gafney HD, Redel E (2015) An experimental and theoretical approach to understanding the surface properties of one-dimensional TiO₂ nanomaterials. *J Phys Chem C* 119(34):19729–19742. <https://doi.org/10.1021/acs.jpcc.5b02027>
- Sharma D, Parveen K, Oza A, Ledwani L (2018) Synthesis of anthraquinone-capped TiO₂ nanoparticles using R. emodi roots: preparation, characterization and cytotoxic potential. *Rend Lincei* 48(6):594–600. <https://doi.org/10.1007/s12210-018-0696-5>
- Sofianou MV, Trapalis C, Psycharis V, Boukos N, Vaimakis T, Yu J, Wang W (2012) Study of TiO₂ anatase nano and microstructures with dominant {001} facets for NO oxidation. *Environ Sci Pollut Res* 19:3719–3726. <https://doi.org/10.1007/s11356-012-0747-x>
- Sunada K, Watanabe T, Hashimoto K (2003) Studies on photokilling of bacteria on TiO₂ thin film. *J Photochem Photobiol A Chem* 156(1–3):227–233. [https://doi.org/10.1016/S1010-6030\(02\)00434-3](https://doi.org/10.1016/S1010-6030(02)00434-3)
- Tian F, Zhang Y, Zhang J, Pan C (2012) Raman spectroscopy: a new approach to measure the percentage of anatase TiO₂ exposed (001) facets. *J Phys Chem C* 116(13):7515–7519. <https://doi.org/10.1021/jp301256h>
- Vinković Vrček I, Pavičić I, Cmković T, Jurašin D, Babić M, Horák D, Lovrić M, Ferhatović L, Čurlin M, Gajović S (2015) Does surface coating of metallic nanoparticles modulate their interference with in vitro assays? *RSC Adv* 5:70787. <https://doi.org/10.1039/c5ra14100a>
- Wamer WG, Yin JJ, Wei RR (1997) Oxidative damage to nucleic acids photosensitized by titanium dioxide. *Free Radic Biol Med* 23(6):851–858. [https://doi.org/10.1016/S0891-5849\(97\)00068-3](https://doi.org/10.1016/S0891-5849(97)00068-3)
- Wang Y, Cui H, Zhou J, Li F, Wang J, Chen M, Liu Q (2015) Cytotoxicity, DNA damage, and apoptosis induced by

- titanium dioxide nanoparticles in human non-small cell lung cancer A549 cells. *Environ Sci Pollut Res* 22:5519–5530. <https://doi.org/10.1007/s11356-014-3717-7>
- Wright C, Iyer AK, Wang L, Wu N, Yakisich JS, Rojanasakul Y, Azad N (2017) Effects of titanium dioxide nanoparticles on human keratinocytes. *Drug Chem Toxicol* 40(1):90–100. <https://doi.org/10.1080/01480545.2016.1185111>
- Yoshizumi M, Nakamura T, Kato M, Ishioka T, Kozawa K, Wakamatsu K, Kimura H (2008) Release of cytokines/chemokines and cell death in UVB-irradiated human keratinocytes, HaCaT. *Cell Biol Int* 32:1405–1411. <https://doi.org/10.1016/j.cellbi.2008.08.011>
- Zeni PF, Dos Santos DP, Canevarolo RR, Yunes JA, Padilha FF, Júnior RLC, Egues SM, Hernández-Macedo ML (2018) Photocatalytic and cytotoxic effects of nitrogen-doped TiO₂ nanoparticles on melanoma cells. *J Nanosci Nanotechnol* 18: 3722–3728. <https://doi.org/10.1166/jnn.2018.14621>

Publisher's note Springer Nature remains neutral with regard to jurisdictional claims in published maps and institutional affiliations.